The Journal of Experimental Biology 212, 3490-3498
Published by The Company of Biologists 2009
doi:10.1242/jeb.033050

Kinematics of suction feeding in the seahorse *Hippocampus reidi*

Gert Roos[1,*], Sam Van Wassenbergh[1], Anthony Herrel[1,2] and Peter Aerts[1,3]

[1]Department of Biology, University of Antwerp, Universiteitsplein 1, B-2610 Antwerpen, Belgium, [2]UMR 7179 CNRS/MNHN Département d'Ecologie et de Gestion de la Biodiversité, 57 rue Cuvier, Case postale 55, 75231, Paris Cedex 5, France and [3]Department of Movement and Sports Sciences, Ghent University, Watersportlaan 2, B-9000 Gent, Belgium

*Author for correspondence (gert.roos@ua.ac.be)

Accepted 14 July 2009

SUMMARY

Fish typically use a rostro-caudal wave of head expansion to generate suction, which is assumed to cause a uni-directional, anterior-to-posterior flow of water in the expanding head. However, compared with typical fish, syngnathid fishes have a remarkably different morphology (elongated snout, small hyoid, immobile pectoral girdle) and feeding strategy (pivot feeding: bringing the small mouth rapidly close to the prey by neurocranial dorsorotation). As a result, it is unclear how suction is generated in Syngnathidae. In this study, lateral and ventral expansions of the head were quantified in *Hippocampus reidi* and linked to the kinematics of the mouth, hyoid and neurocranium. In addition, the flow velocities inside the bucco-pharyngeal cavity and in front of the mouth were calculated. Our data suggest that the volume changes caused by lateral expansion are dominant over ventral expansion. Maximum gape, neurocranium rotation and hyoid depression are all reached before actual volume increase and before visible prey movement. This implies that, unlike previously studied teleosts, hyoid rotation does not contribute to ventral expansion by lowering the floor of the mouth during prey capture in *H. reidi*. The lateral volume changes show a rostro-caudal expansion, but the maximal flow velocity is not near the mouth aperture (as has been demonstrated for example in catfish) but at the narrow region of the buccal cavity, dorsal to the hyoid.

Key words: Syngnathidae, suction feeding, volume changes, flow velocity.

INTRODUCTION

Feeding by means of suction is common in aquatic vertebrates such as teleost fish (Muller and Osse, 1984; Ferry-Graham and Lauder, 2001; Gibb and Ferry-Graham, 2005) and elasmobranchs (Wilga et al., 2007). This feeding mode consists of a rapid and coordinated expansion of the buccal cavity in order to generate a flow of water from the environment in front of the fish's head towards and into the mouth opening (Lauder, 1985). Faster and larger buccal expansion increases suction performance (Muller et al., 1982; Higham et al., 2006a; Higham et al., 2006b; Holzman et al., 2007), but requires higher power output from the muscles responsible for buccal expansion (Carroll and Wainwright, 2006; Coughlin and Carroll, 2006; Van Wassenbergh et al., 2006a).

Recent studies have shown that the epaxial and hypaxial musculature are responsible for delivering the largest fraction of total suction power in fish (Carroll et al., 2004; Carroll and Wainwright, 2006; Coughlin and Carroll, 2006; Van Wassenbergh et al., 2008). Contraction of these muscles causes an increase in the angle between the neurocranium and the pectoral girdle and, indirectly, this results in buccal expansion through a ventro-caudal rotation of the hyoid apparatus [e.g. four-bar model by Muller (Muller, 1987)], which pushes the bottom of the buccal cavity away from the roof of the buccal cavity. Furthermore, the ventro-caudal rotation of the hyoid apparatus can co-occur with abduction of the left and right hyoid rami, which pushes the suspensoria outwards (Muller, 1989; Aerts, 1991; De Visser and Barel, 1996). As a result, the epaxial and hypaxial muscles can also be indirectly responsible for powering the widening of the buccal cavity (i.e. suspensorium abduction).

Even though syngnathid fishes [pipefish, seahorses and close relatives (Kuiter, 2003)] are specialised suction feeders (Bergert and Wainwright, 1997; de Lussanet and Muller, 2007; Van Wassenbergh et al., 2008; Roos et al., 2009) the hyoid apparatus is strongly reduced in size, despite its crucial role in buccal expansion in most fish. For example, the length of the hyoid apparatus in the seahorse *Hippocampus reidi* equals only 15% of the total head length (Roos et al., 2009); in other suction-feeding fish this proportion typically varies between 20 and 60% (Gibb, 1997). Furthermore, hyoid rotation proceeding beyond its maximal depression (i.e. dorso-caudal hyoid rotation) has been observed in seahorses (Roos et al., 2009) and manipulation of preserved *H. reidi* specimens showed a considerable widening of the snout (consisting of the elongated suspensorial bones) co-occurring with posterior rotation of the hyoid and depression of the lower jaws. Given the unusual morphology and kinematics of the hyoid apparatus, it is questionable how buccal expansion is achieved in syngnathid fish as it appears that the hyoid's original suction-generating role has been modified in the evolutionary history of Syngnathoidei.

Muller (Muller, 1987) postulated that the hyoid apparatus of syngnathid fish is part of a lock-and-trigger mechanism, which allows a catapult-like mechanism of neurocranial dorsorotation: when the hyoid complex is kept in a locked position, contraction of the epaxial and hypaxial muscles will lengthen the tendons of the epaxial and hypaxial musculature, allowing syngnathids to store elastic energy. When the hyoid complex is brought out of its locked position, the previously stored elastic energy will suddenly be released, resulting in a very fast rotation of the hyoid complex and the neurocranium. This hypothesis was recently validated for the pipefish *Syngnathus leptorhynchus* (Van Wassenbergh et al., 2008; Van Wassenbergh and Aerts, 2009).

The aims of this study were twofold: our first goal was to test whether the hyoid complex has an important role in depressing the

floor of the buccal cavity in the syngnathid representative *H. reidi*. To do so, we quantified the contribution of depression of the floor of the buccal cavity to the total buccal expansion in *H. reidi*. Second, we analysed flow velocity patterns in front of and inside the mouth using models and evaluated the potential consequences thereof for prey transport. Unlike typical teleost suction feeders, sygnathid fish are characterised by a remarkably narrow and long buccal cavity. Since the shape of the buccal cavity is likely to have important consequences for the velocity of the water flow as a result of expansion of the buccal cavity, it is important to understand how head expansion kinematics relate to fluid flow speeds in the seahorse *H. reidi*. These flow speeds can be calculated by mathematical models based on measured prey capture kinematics of *H. reidi*.

MATERIALS AND METHODS

Study species

Two individuals of the seahorse species *H. reidi* Ginsburg 1933 were obtained through the commercial pet trade. The head lengths (measured from the snout tip to the caudal tip of the operculum) of the two animals were similar: 34.0 mm for the first individual and 32.7 mm for the second individual. The seahorses were kept in a large aquarium (200 l) at a constant temperature of 24°C, constant salinity of 35 p.p.t. and natural photoperiod, and were fed defrosted *Neomysis vulgaris* daily. For filming sessions, the animals were transferred to a smaller aquarium (30 l). The seahorses were trained to capture prey (defrosted *N. vulgaris*) in a narrow section of this aquarium to increase the chances of filming the animals positioned at an angle perpendicular to the camera. Prey items were offered in this narrow section.

High-speed video recordings

As mentioned in the Introduction, suction feeding is a three-dimensional phenomenon. In previous studies (e.g. Muller and Osse, 1984; Van Wassenbergh et al., 2006a), movements of the feeding apparatus in the lateral and ventral plane were often simultaneously recorded with one camera using a mirror at 45 deg. relative to the bottom of the tank. Unfortunately, attempts to use this technique failed because of a significant loss of sharpness owing to depth of field problems related to the seahorse's typical morphology and strong dorsorotation of the neurocranium during suction. Since only one camera was available that could reach a sufficiently high frame rate (4000 frames s^{-1}), we were forced to film the dorsal and lateral view videos separately.

Videos were recorded with a digital high-speed camera (Redlake Motionscope M3, Redlake Inc., Tallahassee, FL, USA) with a recording speed of 4000 frames s^{-1} and shutter time of 0.10 µs. Four arrays of eight red ultra-bright LEDs were used for illumination. Out of all lateral view recordings, only those with the lateral side of the head orientated perpendicular to the camera lens axis were retained for further analysis. For the dorsal view recordings, only videos in which the head moved in the vertical plane were used for analysis. For each individual, five dorsal and five lateral view videos were analysed.

In the lateral view videos, time=0 ms was defined as one time frame prior to the onset of hyoid rotation. Here we use hyoid rotation as the rotation of the entire hyoid complex consisting of the ceratohyals, interhyals and basihyals (Roos et al., 2009), and we use this terminology throughout the manuscript. Since hyoid rotation was not visible in the dorsal view videos, the average time difference between the onset of hyoid rotation and the onset of cranial rotation (a measurement showing very little strike-to-strike variation: s.d.=0.13 ms), as measured from the lateral view videos, was used to set time zero for the dorsal view videos. The onset of neurocranial rotation could be successfully determined from the change in the projected head length to the video plane, allowing the temporal alignment of lateral and dorsal view videos.

To justify the combination of the lateral and dorsal view videos, the time between the onset of cranial rotation and maximum cranial rotation was determined for each of the analysed lateral and dorsal view recordings. Next an analysis of variance (ANOVA) was performed to test whether the measured time difference was significantly different for the two views (dorsal and lateral), and for the two individuals. The results of the ANOVA show no statistical difference between the dorsal and lateral view and between individuals (two-way ANOVA, $F_{3,16}$=0.94, P=0.45).

Volume and flow velocities

The ellipse method for calculating the volume of biological objects was established and validated by Drost and van den Bogaart (Drost and van den Bogaart, 1986). They showed that the accuracy of their method was sufficient for a wide range of biological applications, and even provided a test of their model specifically for the case of calculating flow velocities in a suction-feeding fish. A second validation of the model was done in suction-feeding turtles (Aerts et al., 2001), where calculated flow velocities were compared with measured velocities of a small, freely suspended prey. We feel that these two independent validations, together with the fact that the cross-sectional shape of the head of a seahorse approximates an ellipse at most locations, allows us to safely rely on this method for calculating flow velocities inside the seahorse's buccal cavity. In practice, this model represents the seahorse head (from the tip of the snout to the distal tip of the operculum) by a series of 21 elliptical cylinders, of which the short axis of the ellipse surface corresponds with the width of the head, the long axis corresponds with the height of the head, and the height of the cylinder is equal for each cylinder and is defined as the length of the head divided by 21 (Fig. 1).

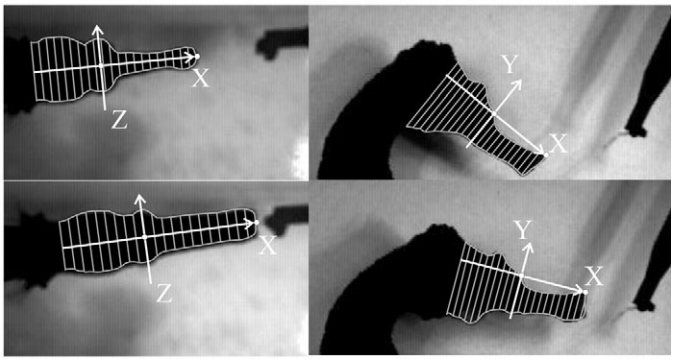

Fig. 1. Example of the expanding ellipse model by Drost and van den Bogaart (Drost and van den Bogaart, 1986) applied to a seahorse head. The left-hand pictures are examples of the dorsal view video recordings of the unexpanded (upper left) and expanded (lower left) seahorse head. The *X*-axis of the fish-bound frame of reference is the line connecting the middle of the snout with the middle of the eyes and reaching the end of the operculum. On the right-hand side examples of the lateral view video recordings of the unexpanded (upper right) and expanded (lower right) head are shown. The *X*-axis is the line connecting the snout tip with the middle of the eye. For each time step, the fish-bound frame of reference is determined and the contour lines of the head digitised. The head (from the tip of the snout to the distal tip of the operculum) is divided into 21 intervals of equal length. Using linear interpolations the height and width of the head at each interval at each time step were determined.

A fish-bound frame of reference was determined for each frame of each video. In the lateral view recordings, the *X*-axis was defined as the line connecting the snout tip and the centre of the eye. The centre of the eye was defined as the origin of the reference frame. In the dorsal view videos, the *X*-axis was determined analogously as the line connecting the middle of the snout tip with the centre of the eyes (Fig. 1). Next, the coordinates of the contours of the head were digitised frame by frame for each video using 50 landmarks in total for each frame, with 25 at each side of the head for the dorsal view videos, and 25 each at the dorsal and ventral side of the head for the lateral view videos. For the lateral view videos, 21 distances between the ventral and the dorsal side of the head and perpendicular to the *X*-axis were calculated for each frame using linear interpolations. Similarly, 21 distances between the left and right side of the head and perpendicular to the *X*-axis were calculated for each frame of the dorsal view videos. The 21 extracted heights and widths for each frame were filtered with a fourth-order low-pass zero phase shift Butterworth filter with a cut-off frequency of 200 Hz to reduce noise caused by digitisation.

Because the different views were not recorded simultaneously, the means of the 21 heights and widths were calculated for each time step from the 10 dorsal and 10 lateral view videos. This results in 21 average ellipse cross-sectional surfaces for each instant. Multiplying each ellipse surface by the mean height of the cylinder (the total length of the *X*-axis divided by 21) for each frame, the volume of each cylinder at each time instant was obtained. Summation of the volumes of all cylinders gives the total, instantaneous head volume.

When the 21 distances between the dorsal and the ventral side (i.e. the head height) are kept constant and equal to their initial value during the analysis, the calculated change in volume during the feeding event is caused by lateral expansion only. The volume calculations during this analysis, therefore, represent the lateral volume contribution. Similarly, keeping the distances between the left and right side of the head (i.e. head width) constant and equal to their initial value during the analysis gives the volume change due only to dorso-ventral expansion and these changes represent the dorso-ventral volume contribution.

The initial volume of the internal bucco-pharyngeal cavity was obtained through X-ray imaging (40 kV, 10 mA, portable X-ray, type AJEX9020H, AJEX Meditech Ltd, Kyunggi-do, Korea) of the dorsal and lateral side of an unexpanded head of a defrosted specimen with a head size similar to that of the specimens used for video recording (33.07 mm). To visualise the bucco-pharyngeal cavity on the X-ray image, an opaque fluid (saturated barium solution) was poured into the seahorse's mouth, allowing us to accurately determine the boundaries of the bucco-pharyngeal cavity. As for the outer contours, the cavity was represented by a series of 21 elliptical cylinders and the heights and widths of the cylinders were calculated in the same way as described above. Subsequently, the volume of each cylinder was calculated, providing the volume of the buccal cavity prior to the onset of the feeding strike.

When the volume of the head tissue is assumed to remain constant, each volume change, as deduced from the outer contours, must be equal to the volume change of the bucco-pharyngeal cavity. Because of the law of continuity, each volume increase of the bucco-pharyngeal cavity must be filled immediately with water. The instantaneous flow velocity at any cross-sectional level of the mouth cavity was calculated as the volume change of the cavity posterior to that cross-section divided by the cross-sectional surface, multiplied by the time interval. These calculations are valid as long as the opercular valves remain closed (i.e. zero flow at the opercular slits) (Muller et al., 1982; Muller and Osse, 1984; Drost and van den Bogaart, 1986). The flow velocity in front of the mouth opening was calculated using the formula presented by Muller et al. (Muller et al., 1982) and recently shown to be accurate (Day et al., 2005; Van Wassenbergh et al., 2006a):

$$v = \frac{(v_{\mathrm{m}} h^3)}{(d^2 + h^2)^{1.5}} , \qquad (1)$$

where v is the velocity of the water in front of the mouth opening in the direction of the longitudinal *X*-axis, v_{m} is the flow velocity at the mouth opening, h is the radius of the mouth opening (calculated as the root of the sum of the square of half the height of the mouth opening and the square of half the width of the mouth opening) and d is the distance along the longitudinal *X*-axis at which the flow velocity is calculated. All velocities are thus expressed in the fish-bound frame of reference. Spatio-temporal patterns of flow velocities are presented as contour plots, in which an anterior-to-posterior flow of water is defined as a positive flow velocity.

Transport of a small prey inside the buccal cavity along the longitudinal axis was simulated using the obtained spatio-temporal flow pattern. It was assumed that the prey moves as a water particle (see also van Leeuwen and Muller, 1984; Drost and van den Bogaart, 1986; Van Wassenbergh et al., 2006a). During this simulation, the prey entered the mouth at the average time the mysid shrimp entered the mouth *in vivo*. Numerical integration (time step=0.25 ms) of the local and instantaneous flow velocity along the centre line yielded prey displacement. The simulation was stopped when the prey reached the back of the head.

Kinematic variables

In the lateral view videos the following landmarks were digitised frame by frame (Didge, version 2.2.0, A. Cullum, Creighton University, Omaha, NE, USA) (Fig. 2A): (1) the tip of the snout near the premaxilla, (2) the dorsal ridge on the frontal bone, located just anterior to the eye, (3) the tip of the lower jaw, (4) the approximate lower jaw joint, (5) the symphysis of the ceratohyals, (6) the point where the ceratohyal intersects the ventral boundary of the snout (interopercular bone) and (7) the eye of the prey. With these landmarks five kinematic variables were calculated as a function of time: (i) gape distance (distance 1–3), (ii) gape angle (angle 3–4–6), (iii) the difference in neurocranium angle (angle between 1 and 2, the horizontal minus the starting angle of the neurocranium), (iv) hyoid angle (angle 4–5–6) and (v) the distance

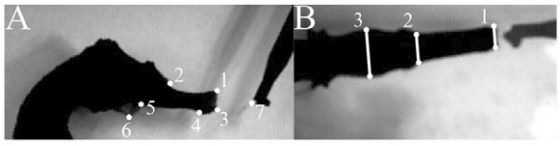

Fig. 2. (A) The seven digitised landmarks in the lateral view video recordings used to calculate mouth opening, and neurocranium and hyoid rotation. (1) The tip of the snout near the premaxilla, (2) the dorsal ridge on the frontal bone, located just anterior to the eye, (3) the tip of the lower jaw, (4) the approximate lower jaw joint, (5) the symphysis of the ceratohyals, (6) the point where the ceratohyal intersects the ventral boundary of the snout (interopercular bone) and (7) the eye of the prey. (B) The three digitised landmarks on each side of the head for calculation of distances at three different positions along the head. (1) The anterior part of the upper jaw, (2) the end of the snout, anterior to the eye and (3) the middle of the operculum.

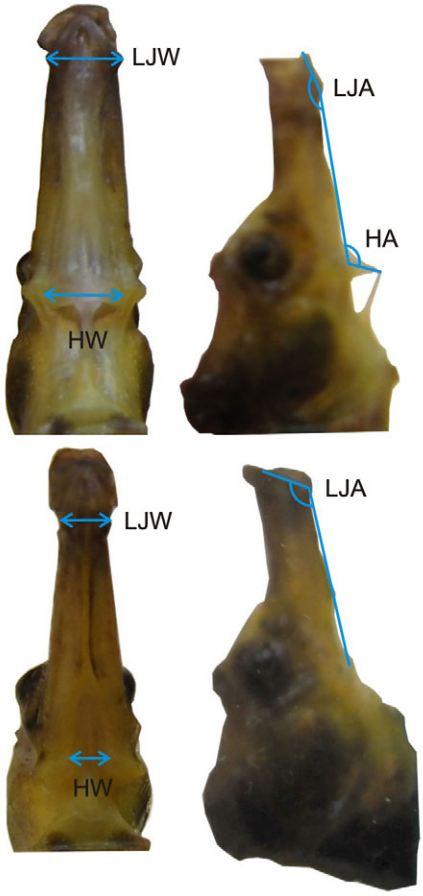

Fig. 3. Representative photographs of the manipulation experiments with the ventral view (left) and lateral view (right) of the expanded (top) and unexpanded (bottom) seahorse head. The four determined variables are lower jaw angle (LJA), hyoid angle (HA), lower jaw width (LJW) and hyoid width (HW). Note that the hyoid angle of the unexpanded lateral view picture is not shown because the hyoid complex is not retracted and therefore the hyoid angle equals zero.

of the prey relative to the middle of the mouth (distance 1,3–7). To test whether the feeding behaviour differs significantly between individuals, ANOVAs were conducted for the peak value of each variable and for every time to peak value.

In the dorsal view videos three landmarks on each side of the head were digitised (Fig. 2B): (1) the anterior part of the upper jaws, (2) the end of the snout, just anterior to the eyes and (3) the middle of the opercular bone. The distances between the corresponding landmarks were calculated to extract the widths as a function of time at three different positions along the head.

To reduce the digitisation noise, the kinematic variables were filtered with a fourth-order zero phase shift Butterworth filter with a low-pass cut-off frequency of 1000 Hz and for one frame of a feeding event (for the lateral view and for the dorsal view); the kinematic variable and volumes were analysed 10 times to quantify the accuracy of these measurements. The mean and standard error were calculated for these variables and divided by the average value of the respective variable to obtain the percentage digitising error.

Manipulation experiment

To investigate the relationship between hyoid rotation, mouth opening and the suspensorial bone movement more quantitatively, manipulation experiments were conducted. Two seahorse (*H. reidi*) specimens were killed with an overdose of MS-222 and a few minutes later the body was clamped and orientated with the ventral side of the head upwards. The camera lens was positioned perpendicular to the ventral side of the head. A mirror was placed at an angle of 45 deg., through which the lateral side of the head was simultaneously visible. With forceps, the ceratohyals were manually placed in different angles and pictures were taken. Digitisation software was used to locate eight anatomical features on every picture. On the lateral view of the head, four landmarks were digitised: (1) the tip of the lower jaw, (2) the articulating point of the lower jaw, (3) the symphysis of the ceratohyals and (4) the articulating point of the ceratohyals, near the interhyals. On the ventral view, four landmarks were analysed: (5,6) the two articulating points of the lower jaw and (7,8) the two articulating points of the ceratohyals, near the interhyals. A total of four variables (Fig. 3) were extracted from the digitisation analysis: the lower jaw angle (angle 1–2–4) and the hyoid angle (angle 2–4–3) were obtained from the lateral view and the hyoid width (distance 5–6) and the lower jaw width (distance 7–8) were extracted from the ventral view photographs. The lower jaw and hyoid angle, obtained through manipulation and video recordings, were plotted in relation to each other. Additionally, for the manipulation data, the hyoid width and the jaw width were plotted relative to the hyoid angle.

RESULTS

Kinematics

The maximum percentage digitising error for the kinematic variables was 1.09% and thus kinematic data are presented using three significant figures. Furthermore, no kinematic variable was significantly different between the two individuals (Table 1) allowing us to combine their data. The feeding strike was always initiated by the onset of hyoid rotation. At 0.4±0.1 ms (mean ± s.d., N=10) the neurocranium started to rotate dorsally and at 0.7±0.1 ms mouth opening began. Peak gape of 4.43±0.89 mm was reached first, at 2.6±0.4 ms (Fig. 4C), followed by peak gape angle of 159±8 deg. at 3.0±1.3 ms (Fig. 4D), maximal neurocranium rotation of 26.7±8 deg. at 3.6±2.3 ms (Fig. 4B, black line, T_1) and maximal hyoid rotation of 118±18 deg. at 19.6±3.0 ms (Fig. 4A). The hyoid reached an angle of 90 deg. at 1.2±0.2 ms. The prey started to move at 4.0±0.5 ms (Fig. 4, yellow line, T_2) at which time the distance of the prey to the mouth was equal to 0.76±0.09 of the average maximal gape height (Fig. 4F), and the prey crossed the gape at 5.7±0.8 ms (Fig. 4F, red line, T_3). In the dorsal view videos, the anterior part of the upper jaws expanded first at 2.0±0.3 ms (Fig. 4E). Next the posterior part of the snout started to expand at 2.5±0.9 ms (Fig. 4E) and at 4.8±1.7 ms (Fig. 4E) the opercula started to widen. The individual results of the kinematic study and the analysis of variance for each variable between individuals are presented in Table 1.

Manipulation experiment

During the manipulation experiment, the lower jaw started to rotate the moment the hyoid complex was retracted (Fig. 5A, black graph), resulting in a jaw angle excursion of 20 deg. for a hyoid angle of only 4 deg. After this initial phase, the lower jaw continued to rotate slowly with increasing hyoid angle. When the hyoid angle approximated 90 deg., the jaw angle suddenly increased and continued to do so as the hyoid angle increased. The jaw angle obtained from the video recordings remained the same for a hyoid rotation of 60 deg. (Fig. 5A, grey graph). When the hyoid angle passed the 80 deg. mark, the jaw angle started to increase and continued to do so up to a hyoid angle of 120 deg., at which point the jaw angle started to decrease.

Table 1. The results of the kinematic analysis for each individual combined with an analysis of variance testing for differences between individuals

Variable	Individual 1 (means ± s.d. *N*=5)	Individual 2 (means ± s.d. *N*=5)	$F_{1,9}$	*P*
Peak hyoid angle (deg.)	123±15	109±17	2.73	0.12
Time to peak hyoid angle (ms)*	20.0±2.9	20.5±3.3	0.10	0.76
Time to 90 deg. hyoid angle (ms)*	1.2±0.3	1.3±0.6	0.20	0.66
Onset of neurocranial rotation (ms)*	0.4±0.1	0.4±0.1	0.52	0.82
Peak neurocranium angle (deg.)	28.0±9.4	24.6±3.1	0.60	0.46
Time to peak neurocranium angle (ms)*	4.7±2.2	6.2±2.3	1.36	0.27
Onset of mouth opening (ms)*	1.6±0.1	1.6±0.1	0.14	0.72
Peak gape distance (mm)	4.3±1.1	4.6±0.3	0.32	0.58
Time to peak gape (ms)*	3.5±0.3	3.7±0.3	0.52	0.49
Peak gape angle (deg.)	161±5	159±4	0.59	0.46
Time to peak gape angle (ms)*	2.7±0.5	2.8±0.3	0.04	0.84
Onset of prey movement (ms)*	4.0±0.5	4.0±0.6	0.05	0.83
Time at which prey enters the mouth (ms)*	5.8±0.7	5.7±0.8	0.05	0.83
Time to peak jaw width (ms)*	2.0±0.7	2.0±0.5	0.02	0.89
Time to peak posterior snout width (ms)*	2.5±0.7	2.8±0.7	0.35	0.57
Time to peak opercula width (ms)*	4.7±0.5	4.9±0.5	0.23	0.65

*Time=0 ms is one frame prior the onset of hyoid rotation.

Over the first 20 deg. of hyoid rotation caused by manipulation, the width of the jaw and hyoid increased strongly (Fig. 5B). Between a hyoid rotation of 20 deg. and 90 deg. both widths continued to increase but more slowly. After 90 deg. of hyoid rotation, the hyoid width suddenly increased and continued to increase greatly with increasing hyoid angle (Fig. 5B). The jaw angle also increased faster, but not as fast as the hyoid width (Fig. 5B).

Volume changes and flow velocities

The digitising error found for the volume calculations was 0.37%. The initial volume of the buccal cavity equalled 550 mm^3 (100%). At 1.0 ms buccal compression started and became minimal (512 mm^3, 94%) at 4.0 ms (Fig. 6, upper and middle panel). From that moment on, buccal expansion started. Total volume increase was 147 mm^3, which was reached after 18.3 ms. At this instant, the buccal volume equalled 660 mm^3 (120%).

When only considering the volume change due to ventral expansion, our models showed that the volume increases by 66 mm^3, reaching this maximum after 3.8 ms (Fig. 7, upper panel). Looking at the spatial component of these volume changes, the increase in volume occurred in three regions: at the level of the mouth, the hyoid complex and the pectoral girdle (Fig. 7, lower panel).

Our calculation of volume changes due only to lateral expansion showed a decrease of 97 mm^3 in the first 4.0 ms. Thereafter, the volume increase due to lateral expansion was 148 mm^3 at 17.8 ms (Fig. 8, upper panel). The large decrease in the initial 4.0 ms was found at the level of the opercula. At 2.5 ms, the snout started to expand laterally and at 4.8 ms the opercula started to abduct (Fig. 8, lower panel).

The opercular siphons opened for a short duration between 1.5±0.3 ms and 5.6±0.9 ms (Fig. 6, lower panel, grey zone). After closing of the siphons, the expansion of suspensorium and operculum continued. Note that the closure of the siphons coincided with the instant at which the prey entered the mouth. As mentioned in Materials and methods, flow velocities cannot be calculated when the jaws and opercular siphons are open simultaneously. The transparent grey zone in the lower panel of Fig. 6 represents the time interval at which the system is mathematically undetermined. The contour plot behind the transparent grey zone represents the flow velocities inside the buccal cavity when assuming no outflow at the level of the opercular siphons.

Because of the large volume decrease at the level of the opercula during the initial 4.0 ms (Fig. 8), the flow velocity inside the buccal cavity was negative with a peak value of –2.87 $m\,s^{-1}$ at 1.5 ms just before the opercular valves opened (Fig. 6). Right after the siphons closed again, the flow velocity was positive with a maximum value of 3.17 $m\,s^{-1}$ at 7.0 ms at the opercular level (Fig. 6, lower panel).

Prey transport

The shrimps started to move at 4.0±0.5 ms and entered the mouth at 5.7±0.8 ms (Fig. 6, lower panel, red line, T_3). Afterwards, the simulation of prey transport through the buccal cavity showed the highest prey velocity of 2.42 $m\,s^{-1}$ at 7.3 ms (Fig. 6, lower panel, white curve). Next, the prey slowed down and reached the posterior side of the head at 13.5 ms. According to the simulation, a small prey item is transported along the entire length of the head in less than 2 ms.

DISCUSSION

The results of the present study show that the time needed to reach maximal buccal expansion in the seahorse *H. reidi* is relatively short at 14.25 ms (cf. Gibb and Ferry-Graham, 2005). However, the total volume increase (i.e. the difference between minimum and maximum head volume; Fig. 6, upper panel) in *H. reidi* is only 30% of the starting buccal volume, which is relatively small compared with that of other previously studied teleosts (e.g. Grobecker and Pietsch, 1979; Higham et al., 2006a). Yet, because of the elongated, narrow shape of the snout and the small gape, this limited expansion of the buccal cavity induces relatively high flow velocities of the water reaching up to 3.17 $m\,s^{-1}$ [cf. 2–3 $m\,s^{-1}$ for *Chelodina longicollis* (Aerts et al., 2001); 1.7–1.8 $m\,s^{-1}$ for *Clarias gariepinus* (Van Wassenbergh et al., 2006a); 1 $m\,s^{-1}$ for *Lepomis macrochirus* (Day et al., 2005)].

During the initial phase of the strike (time=0–1.5 ms), the model predicts posterior to anterior flows of water inside the buccal cavity and out of the mouth (Fig. 6, lower panel). This outflow of water is caused by opercular adduction (Fig. 8). Because the prey is still relatively far away from the mouth at this instant, the predicted outflow of water probably does not cause the prey to be pushed away from the mouth (prey movement was observed after time=4.0 ms). However, more experimental work is needed to verify the direction and timing of flow calculated in the model during this

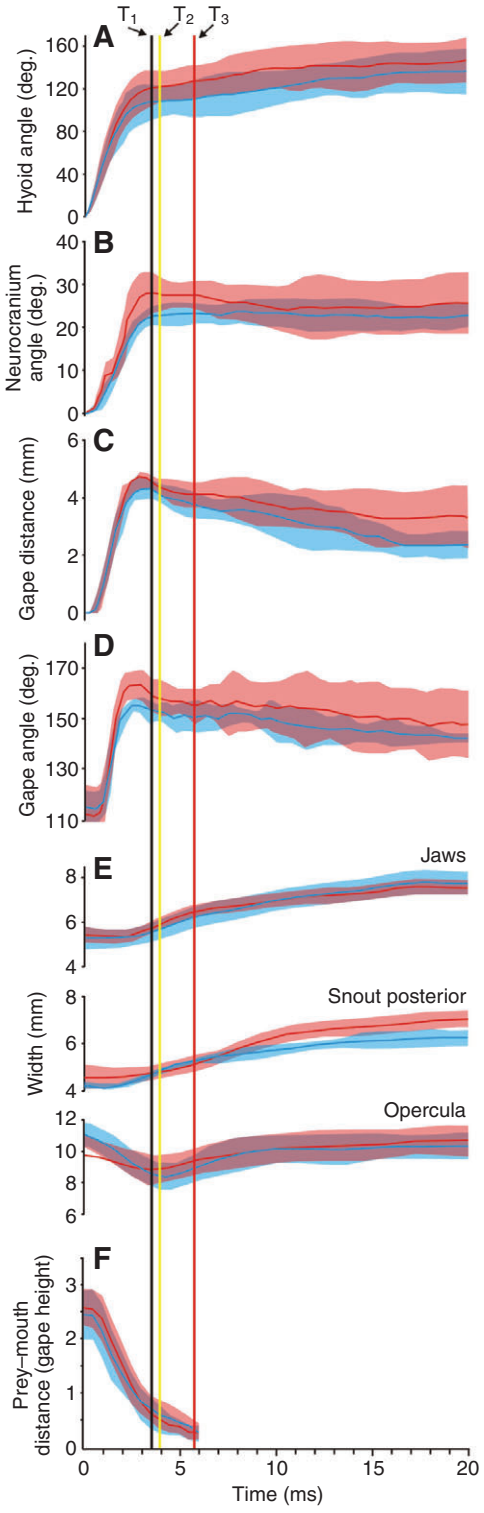

Fig. 4. Mean kinematic profile of individual 1 (*N*=5, red curve) and individual 2 (*N*=5, blue curve) for (A) hyoid rotation, (B) angular displacement of the neurocranium, (C) gape distance, (D) gape angle, (E) width of the anterior part of the upper jaws, the end of the snout anterior to the eyes and the middle of the operculum and (F) distance of the prey relative to the middle of the mouth expressed as maximal gape height. The zone around the profile represents the standard deviation and time=0 ms was defined as one frame prior to the onset of hyoid rotation. The black line (T_1) indicates maximal cranial rotation, the yellow line (T_2) indicates the instant at which the prey started to move, and the red line (T_3) indicates the time at which the prey entered the mouth.

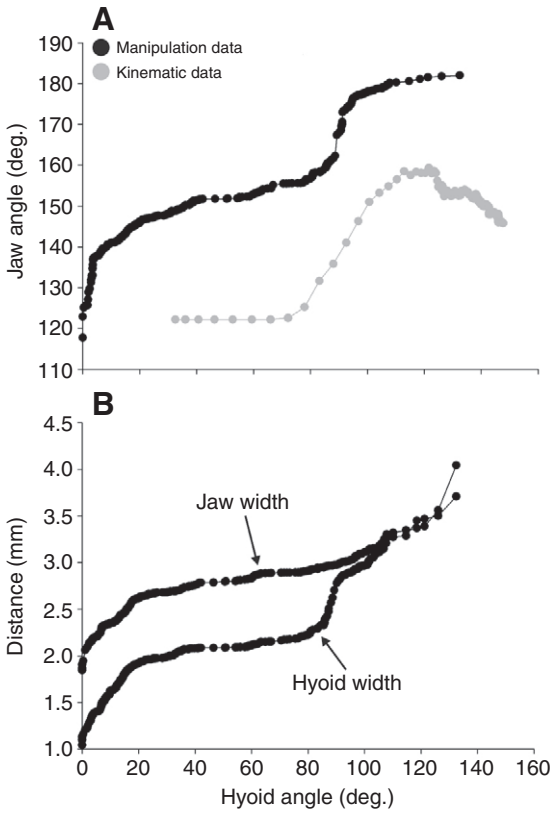

Fig. 5. (A) The kinematic profile of the jaw angle relative to the hyoid angle based on the manipulation experiment (black graph) and on the video recordings (grey graph). Note that the moment the hyoid angle approximates 120 deg., the jaw angle starts to decrease (grey graph); therefore the mouth starts to close (B). This might be the result of contraction of the adductor mandibulae (at that moment functioning antagonistically) to prevent the lower jaw from overstretching. (B) The kinematic profile of the jaw width and the hyoid width relative to the hyoid angle.

early phase of feeding. Since narrowing of the head reduces the head's rotational inertia and hydrodynamic resistance (de Lussanet and Muller, 2007; Van Wassenbergh et al., 2008), the opercular adduction probably increases the velocity of dorsorotation of the head during pivot feeding. The opercular siphons are open between 1.5 and 5.6 ms (Fig. 6, lower panel). Because the mouth is also open during this period, this results in an undetermined model system unless the flow velocity at one of the inflow or outflow openings (i.e. mouth and opercular siphons) is known (Muller et al., 1982; Muller and Osse, 1984; Drost and van den Boogaart, 1986). Unfortunately, this information is not available. Consequently, neither the direction nor the speed of the flow can be inferred from buccal volume changes during this period (note that the calculation results displayed in Fig. 6 represent the situation with no inflow or outflow at the siphons). Although currently unknown, we suggest that the opening of the siphons could be caused by super-ambient pressure inside the buccal cavity resulting from opercular adduction (Fig. 8, lower panel). Additionally, since the opercular region is rapidly accelerated ventro-anteriorly at this stage (Roos et al., 2009), the dorso-posterior outflow of water at the level of the siphons could be the result of the inertia of the water inside the posterior region of the buccal cavity.

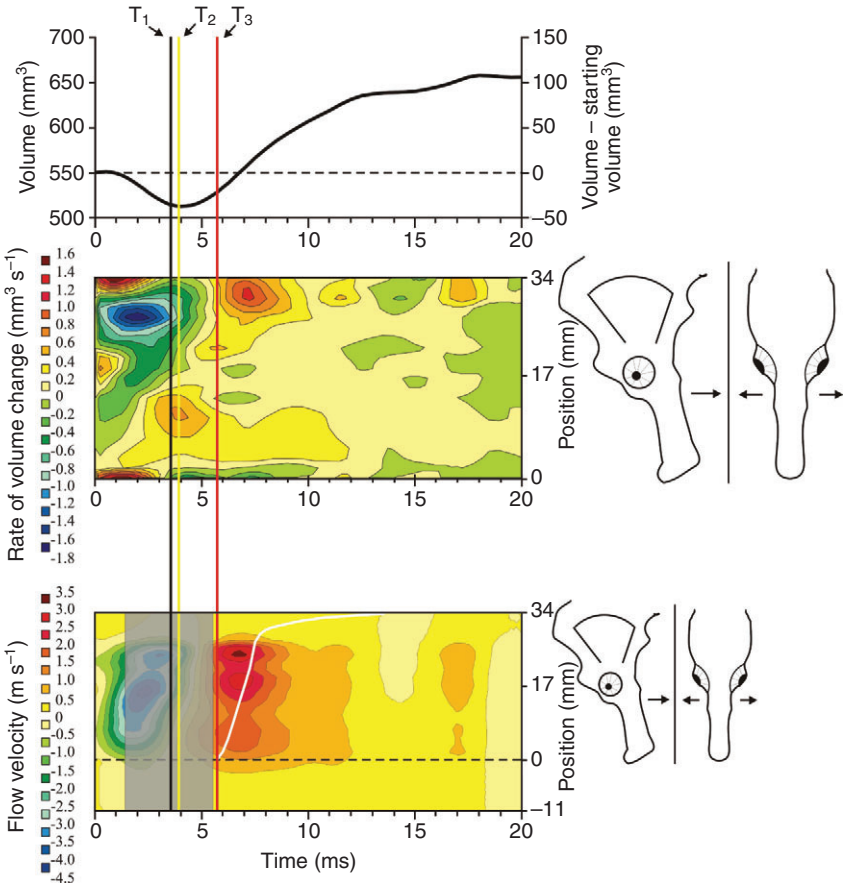

Fig. 6. The total volume change of the bucco-pharyngeal cavity of the seahorse head, with the starting volume indicated by the dashed line (upper panel). The spatio-temporal volume changes are presented in the middle panel. The lower panel shows the flow velocities inside the bucco-pharyngeal cavity relative to time and their position relative to the head (above the dashed line). The portion under the dashed line represents the flow velocities in front of the mouth. Positive flow velocities denote flow in the anterior to posterior direction. The shaded grey zone is the time interval during which the mouth and the opercular siphons are open, hence the system is undetermined. The white curve represents the movement of the prey relative to the head. T_1, T_2, T_3 as in Fig. 5.

During neurocranial rotation, the volume increase due to ventral expansion (Fig. 7, upper panel) can be assigned to three different regions of the head (Fig. 7, lower panel): (1) at the mouth, caused by ventro-caudal rotation of the lower jaws, (2) at the level of the hyoid complex, caused by ventro-caudal rotation of the hyoid and (3) at the end of the head, as additional volume is created between the operculum and the pectoral girdle because of cranial rotation. Nonetheless, the volume increase caused by ventral expansion is fully compensated by lateral compression of the opercula (Fig. 8, lower panel), resulting in a decrease in the total volume during rotation of the neurocranium (Fig. 6, upper panel). This strongly differs from the situation with other suction-feeding fish, where

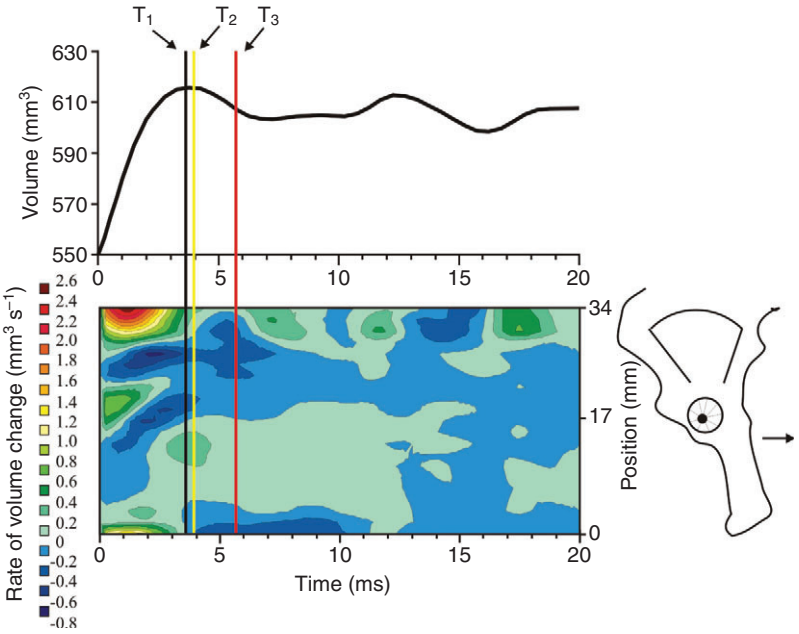

Fig. 7. The upper panel shows the total volume change of the bucco-pharyngeal cavity due only to ventral expansion. The spatio-temporal volume changes solely due to ventral expansion are given in the lower panel, with position 0 mm as the gape. T_1, T_2, T_3 as in Fig. 5.

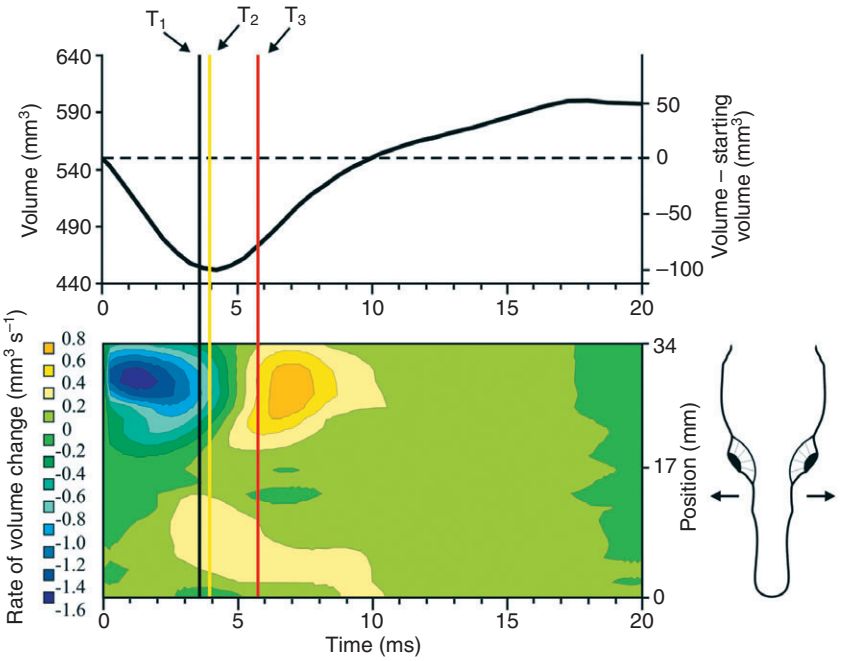

Fig. 8. The volume changes of the bucco-pharyngeal cavity due only to lateral expansion with the starting volume indicated by the dashed line (upper panel). The spatio-temporal volume changes due to lateral expansion are shown in the lower panel, with position 0 mm at the height of the gape. T_1, T_2, T_3 as in Fig. 5.

neurocranial elevation and hyoid depression typically coincide with the major volume increase of the head (e.g. Ferry-Graham and Lauder, 2001).

When maximal cranial rotation is reached (black line, T_1, in Figs 4, 6, 7 and 8), there is no additional ventral expansion anymore (Fig. 7, upper panel). However, from this moment on, the snout begins to expand laterally (Fig. 4E; Fig. 8, lower panel), followed by the abduction of the operculum (Fig. 4E; Fig. 8, lower panel). In contrast to the earlier ventral expansions, these lateral expansions do result in a total volume increase (Fig. 6, upper panel). Therefore, our model suggests that prey transport is achieved after cranial rotation, which seems to be confirmed by the timing of prey motion observed *in vivo*: less than 0.5 ms after maximal rotation of the head, the prey starts to move in the direction of the mouth (Fig. 4F, yellow line, T_2) and at 5.7 ms the prey has entered the mouth (Fig. 4F, red line, T_3). Note, however, that the observed prey motion does not necessarily indicate that suction starts only after maximal neurocranial rotation: suction could begin during neurocranial rotation, but only starts to draw the prey towards the mouth when the distance between the prey and mouth aperture is less than half the maximum gape height (Fig. 4F). Unfortunately, since the opening of the mouth and opercular siphons co-occurs with most of the neurocranial rotation phase, the model was undetermined for that time interval (grey zone, Fig. 6, lower panel). Consequently, to elucidate the flow details during the neurocranial rotation period empirical data based on particle image velocimetry (PIV) recordings are needed.

The ongoing expansion of the suspensorium and the opercula results in relatively high flow velocities, transporting the prey through the snout (Fig. 6, lower panel). Surprisingly, the highest flow velocities are not found near the mouth as typically observed in the suction feeders studied thus far (van Leeuwen and Muller, 1984; Aerts et al., 2001; Van Wassenbergh et al., 2006b) but further inside the buccal cavity. The high flow velocities recorded more posteriorly in the buccal cavity (Fig. 6, lower panel) can be explained by the presence of a narrow region, dorsal to the hyoid complex, where water is flowing rapidly to fill the volume created by opercular abduction (Fig. 9). The simulation shows an increase in flow velocity when moving anterior–posterior in the head, which could result in an acceleration of the prey throughout the entire snout.

In contrast to typical teleosts (e.g. Lauder, 1980; Aerts et al., 1991; Gibb and Ferry-Graham, 2005), the function of the hyoid complex to expand the buccal volume *via* depression of the floor of the mouth appears to be limited to the seahorse *H. reidi*. Maximal hyoid depression (i.e. the ceratohyals at 90 deg. relative to the snout) is reached at approximately 1.2 ms (Fig. 4A). After peak depression, the hyoid complex continues to rotate dorso-caudally, which implies a decreasing head volume because the floor of the mouth is elevated. Since the volume increase caused by ventral expansion is fully compensated by lateral compression (Fig. 6, lower panel) and the prey does not move until 4.0 ms, it is clear that the role of ventral expansion in creating suction flow is minimal, or potentially even non-existent. Furthermore, X-ray images of the unexpanded and expanded head of *H. reidi* show that the water filling the buccal cavity does not flow in between the left and right rami upon hyoid depression (Fig. 9). Consequently, no additional volume appears to be directly created by hyoid rotation.

Nevertheless, the hyoid complex still seems to play an important role in generating suction, by abducting the suspensorial bones of

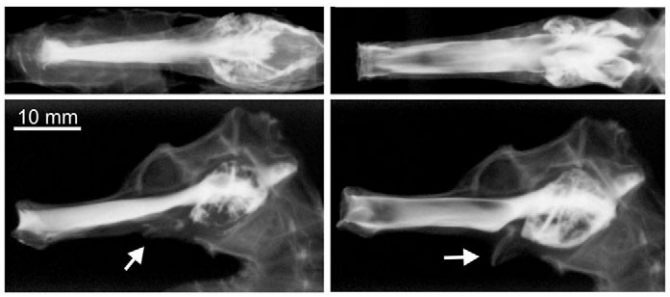

Fig. 9. X-ray images of the dorsal view (top) and lateral view (bottom) of the unexpanded (left) and expanded (right) head. The arrow indicates the position of the ceratohyals. The bright white area presents the bucco-pharyngeal cavity visualised by an opaque barium solution. The scale bar is identical for all images.

the snout as described for more generalised teleosts (De Visser and Barel, 1996). Manually rotating the hyoid in a defrosted specimen automatically results in depression of the lower jaws and abduction of the snout at the level of the jaws and the hyoid complex (Fig. 5). The magnitude of the widening of the snout observed during the manipulation experiment corresponds closely to the *in vivo* maximal snout expansion.

However, the manipulation experiment shows depression of the lower jaw from the moment the hyoid complex starts to rotate, combined with an increase in jaw width and hyoid width (Fig. 5B) while *in vivo* the mouth remains closed during the initial hyoid rotation. Only after the hyoid complex reaches an angle of approximately 80 deg. does the lower jaw start to depress (Fig. 5A, grey graph). Two explanations could account for this closed mouth period: during the start of the strike, the seahorse may actively close the mouth by contraction of the adductor mandibulae muscles. This seems likely, since keeping the mouth closed during initial cranial rotation would prevent the animal from starting suction too early, when the prey is still too far away. Another reason could be a short delay time of the stress propagation from the ceratohyals to the lower jaw in hyomandibular ligaments, which causes the lower jaw to depress when tension reaches the lower jaw (see Roos et al., 2009). For example, if we assume that the tension transmission velocity of the seahorse's hyomandibular ligament (length approximately 10 mm) has the same order of magnitude as measured for resting frog skeletal muscle [about $10\,m\,s^{-1}$ (Moss and Halpern 1977)], a delay of 1 ms can be expected. Indeed, the *in vivo* time differential between the start of hyoid rotation and a hyoid angle of 90 deg. (maximal depression) is only 1.2 ms (Fig. 5A), which approximates the estimated stress-pulse propagation time through the hyomandibular ligament.

Despite the difference in timing of the onset of jaw depression between the *in vivo* situation and the manipulation experiment, the latter shows that only active ventro-caudal rotation of the hyoid is required to generate mouth opening, and jaw and hyoid widening (in other words the expansion of the snout) automatically through a chain of three-dimensional linkages. Since hyoid widening occurs *in vivo* and during manipulation at about the same sagittal plane hyoid angle, which is approximately 90 deg. with respect to the snout, we can infer that this mechanism of transmitting hyoid retraction to snout widening also works *in vivo*. However, despite the fact that the morphology of this linkage system has been described for our study species (Roos et al., 2009), the exact mechanism of force transmission from hyoid retraction to suspensorium abduction remains to be resolved.

In summary, this study addressed the question of how a seahorse, with its specialised head morphology and feeding strategy (pivot feeding), creates suction flow to capture prey. During cranial rotation, the volume increase created because of ventral expansion is fully compensated by the lateral compression of the space between the opercula resulting in a total buccal volume decrease. After neurocranial rotation, the model suggests that suction is generated by lateral expansion of the suspensoria and opercula, and the first prey movement is observed. It is clear that only lateral expansion, and not ventral expansion, has a role in creating suction flow. Consequently, these data suggest that the function of the hyoid complex as a suction generator by depressing the mouth bottom [as in generalised teleosts (Aerts et al., 1991; Gibb and Ferry-Graham, 2005)] is absent. However, since manipulation of preserved specimens showed that hyoid rotation beyond its vertical-most position causes suspensorial abduction, the hyoid complex still plays an important part in suction generation in seahorses.

G.R. is funded by a PhD grant from the Institute for the Promotion of Innovation through Science and Technology in Flanders (IWT-Vlaanderen). S.V.W. is postdoctoral fellow of the Fund for Scientific Research, Flanders (FWO-VI). Supported by FWO-VI grant G 053907. We also thank two anonymous reviewers for their constructive and helpful comments.

REFERENCES

Aerts, P. (1991). Hyoid morphology and movements relative to abducting forces during feeding in *Astatotilapia elegans* (Teleostei: Cichlidae). *J. Morphol.* **208**, 323-345.
Aerts, P., van Damme, J. and Herrel, A. (2001). Intrinsic mechanics and control of fast cranio-cervical movements in aquatic feeding turtles. *Amer. Zool.* **41**, 1299-1310.
Bergert, B. A. and Wainwright, P. C. (1997). Morphology and kinematics of prey capture in the syngnathid fishes *Hippocampus erectus* and *Syngnathus floridae*. *Mar. Biol.* **127**, 563-570.
Carroll, A. M. and Wainwright, P. C. (2006). Muscle function and power output during suction feeding in largemouth bass, *Micropterus salmoides*. *Comp. Bioch. Physiol.* A **143**, 389-399.
Carroll, A. M., Wainwright, P. C., Huskey, S. H., Collar, D. C. and Turingan, R. G. (2004). Morphology predicts suction feeding performance in centrarchid fishes. *J. Exp. Biol.* **207**, 3873-3881.
Coughlin, D. J. and Carroll, A. M. (2006). *In vitro* estimates of power output by expaxial muscle during feeding in largemouth bass. *Comp. Bioch. Physiol.* A **145**, 533-539.
Day, S. W., Higham, T. E., Cheer, A. Y. and Wainwright, P. C. (2005). Spatial and temporal patterns of water flow generated by suction-feeding bluegill sunfish *Lepomis macrochirus* resolved by particle image velocimetry. *J. Exp. Biol.* **208**, 2661-2671.
de Lussanet, M. H. C. and Muller, M. (2007). The smaller your mouth, the longer your snout: predicting the snout length of *Syngnathus acus*, *Centriscus scutatus* and other pipette feeders. *J. R. Soc. Interface* **4**, 561-573.
De Visser, J. and Barel, C. D. N. (1996). Architectonic constraints on the hyoid's optimal starting position for suction feeding in fish. *J. Morph.* **228**, 1-18.
Drost, M. R. and van den Bogaart, J. G. M. (1986). A simple method for measuring the changing volume of small biological objects, illustrated by studies of suction feeding by fish larvae and of shrinkage due to histological fixation. *J. Zool. Lond.* **209**, 239-249.
Ferry-Graham, L. A. and Lauder, G. V. (2001). Aquatic prey capture in ray-finned fishes: a century of progress and new directions. *J. Morphol.* **248**, 99-119.
Gibb, A. C. (1997). Do flatfish feed like other fishes? A comparative study of percomorph prey-capture kinematics. *J. Exp. Biol.* **200** 2841-2859.
Gibb, A. C. and Ferry-Graham, L. A. (2005). Cranial movements during suction feeding in teleost fishes: Are they modified to enhance suction production? *Zoology* **108**, 141-153.
Grobecker, D. B. and Pietsch, T. W. (1979). High-speed cinematographic evidence for ultrafast feeding in antennariid anglerfishes. *Science* **205**, 1161-1162.
Higham, T. E., Day, S. W. and Wainwright, P. C. (2006a). Multidimensional analysis of suction feeding performance in fishes: fluid speed, acceleration, strike accuracy and the ingested volume of water. *J. Exp. Biol.* **209**, 2713-2725.
Higham, T. E., Day, S. W. and Wainwright, P. C. (2006b). The pressures of suction feeding: the relation between buccal pressure and induced fluid speed in centrarchid fishes. *J. Exp. Biol.* **209**, 3281-3287.
Holzman, R., Day, S. W. and Wainwright, P. C. (2007). Timing is everything: coordination of strike kinematics affects the force exerted by suction feeding fish on attached prey. *J. Exp. Biol.* **210**, 3328-3336.
Kuiter, R. H. (2003). *Seahorses, Pipefishes And Their Relatives, A Comprehensive Guide To Syngnathiformes*. Chorleywood, UK: TMC Publishing.
Lauder, G. V. (1980). The suction feeding mechanism in sunfishes (*Lepomis*): an experimental analysis. *J. Exp. Biol.* **88**, 49-72.
Lauder, G. V. (1985). Aquatic feeding in lower vertebrates. In *Functional Vertebrate Morphology* (ed. M. Hildebrand, D. M. Bramble, K. F. Liem, and D. B. Wake), pp. 210-229. Cambridge, MA: Harvard University Press.
Moss, R. L. and Halpern, W. (1977). Elastic and viscous properties of resting frog skeletal muscle. *Biophys. J.* **17**, 213-228.
Muller, M. (1987). Optimization principles applied to the mechanism of neurocranial levation and mouth bottom depression in bony fishes (Halecostomi). *J. Theor. Biol.* **126**, 343-368.
Muller, M. (1989). A quantitative theory of expected volume changes of the mouth during feeding in teleost fishes. *J. Zool. Lond.* **217**, 639-662.
Muller, M. and Osse, J. W. M. (1984). Hydrodynamics of suction feeding in fish. *Trans. Zool. Soc.* London **37**, 51-135.
Muller, M., Osse, J. W. M. and Verhaegen, J. H. G. (1982). A quantitative hydrodynamical model of suction feeding in fish. *J. Theor. Biol.* **95**, 49-79.
Roos, G., Leysen, H., Van Wassenbergh, S., Herrel, A., Jacobs, P., Dierick, M., Aerts, P. and Adriaens, D. (2009). Linking morphology and motion: a test of a four-bar mechanism in seahorses. *Physiol. Biochem. Zool.* **82**, 7-19.
van Leeuwen, J. L. and Muller, M. (1984). Optimum sucking techniques for predatory fish. *Trans. Zool. Soc.* **37**, 137-169.
Van Wassenbergh, S. and Aerts, P. (2009). Rapid pivot feeding in pipefish: flow effects on prey and evaluation of simple dynamic modelling via computational fluid dynamics. *J. R. Soc. Interface* **6**, 149-158.
Van Wassenbergh, S., Aerts, P. and Herrel, A. (2006a). Scaling of suction feeding performance in the catfish *Clarias gariepinus*. *Physiol. Biochem. Zool.* **79**, 43-56.
Van Wassenbergh, S., Aerts, P. and Herrel, A. (2006b). Hydrodynamic modelling of aquatic suction performance and intra-oral pressures: limitations for comparative studies. *J. R. Soc. Interface* **3**, 507-514.
Van Wassenbergh, S., Strother, J. A., Flammang, B. E., Ferry-Graham, L. A. and Aerts, P. (2008). Extremely fast prey capture is powered by elastic recoil. *J. R. Soc. Interface* **5**, 285-296.
Wilga, C. D., Motta, P. J. and Sanford, C. P. (2007). Evolution and ecology of feeding in elasmobranches. *Integr. Comp. Biol.* **47**, 55-69.